ISBN: 978-3-95450-212-7 ISSN: 2673-5482 doi:10.18429/JACoW-CYCLOTRONS2022-MOB003

PROTON IRRADIATION SITE FOR HIGH-UNIFORMITY RADIATION HARDNESS TESTS OF SILICON DETECTORS AT THE BONN ISOCHRONOUS CYCLOTRON

D. Sauerland*, R. Beck, P. D. Eversheim
Helmholtz-Institut f. Strahlen- u. Kernphysik, Bonn, Germany
J. Dingfelder, P. Wolf, Silizium Labor Bonn, Physikalisches Institut, Bonn, Germany

Abstract

The Bonn Isochronous Cyclotron provides proton, deuteron, alpha particle and other light ion beams, having a charge-to-mass ratio $Q/A \geq 1/2$, with kinetic energies in the range of 7 to 14 MeV per nucleon.

At the irradiation site, a 14 MeV proton beam with a diameter of a few mm is used to irradiate detectors, so-called devices under test (DUTs), housed in a thermally-insulated and gas-cooled box. To ensure homogeneous damage application, the DUT is moved through the beam in a row-wise scan pattern with constant velocity and a row separation, smaller than the beam diameter. During irradiation, beam parameters are continuously measured non-destructively using a calibrated, secondary electron emission-based beam monitor, installed at the exit to the site. This allows a beam-driven irradiation scheme, enabling the setup to autonomously react to changing beam conditions, resulting in highly-uniform proton fluence distributions with relative uncertainties of typically 2%.

In this work, the accelerator facility is introduced, the proton irradiation site with focus on its beam diagnostics is presented in detail and resulting fluence distributions are shown.

BONN ISOCHRONOUS CYCLOTRON

The accelerator facility of the Bonn Isochronous Cyclotron is shown in Fig. 1. Here, proton, deuteron, alpha and other light ion beams with kinetic energies of 7 to 14 MeV/A and currents of $\lesssim$ 1 µA, are provided to five experimental sites.

The ion beam is generated by two external electron cyclotron resonance sources: One source (two-stage, 5 GHz) located beside, the other (single-stage, 2.5 GHz, polarized beam) situated underneath the cyclotron. Here, the generated beam with a kinetic energy of 2 to 8 keV is guided through a low-energy beamline below the cyclotron and then is injected vertically into its magnetic center using an electrostatic hyperboloid inflector.

The Bonn Isochronous Cyclotron [1] is an isochronous, three-sector, azimuthally varying field cyclotron. Its main parameters are shown in Table 1. The cyclotron shows a 120°-symmetry in its azimuthal magnetic field pattern due to its magnet yoke being separated into three hill-and-valley sectors with 0° spiral angle. In each valley, a broadband dual-gap dee is located, providing an acceleration voltage of up to 40 kV.

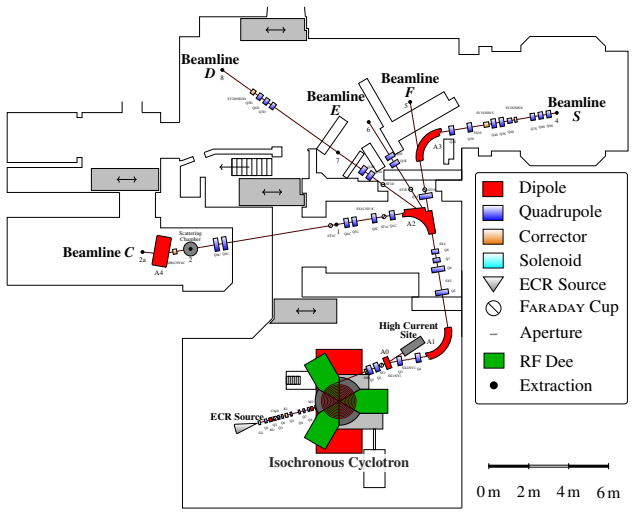

Figure 1: Overview of the accelerator facility.

Table 1: Parameters of the Bonn Isochronous Cyclotron

available ions	p, d, α, …, $^{16}O^{6+}$
energy ($h = 3$, $Q/A \geq \frac{1}{2}$)	7 to 14 MeV/A
beam current (ext.)	$\lesssim$ 1 µA
injection / extraction radius	38 mm / 910 mm
number of revolutions	approx. 120
hill sectors	3 × 40°, 0° spiral angle
hill / valley field strength	1.9 / 0.7 T (max.)
flutter factor	0.62
dees	3 × 40°, 40 kV (max.)
cyclotron harmonic h	3, 9
RF frequency ν_{RF}	20.1 to 28.5 MHz
hor. / vert. emittance	16 / 22 mm mrad
relative energy spread	4×10^{-3}

Due to its symmetry, the cyclotron typically operates at the third cyclotron harmonic $h = 3$, where the RF frequency ν_{RF} equals three times the ions' cyclotron frequency ν_0, but also an operation at $h = 9$ is possible for heavier ions with $Q/A \leq 1/3$. The RF frequency range of 20.1 to 28.5 MHz and the maximum average magnetic flux density $\langle B \rangle_{max}$ of approx. 1.4 T define the cyclotron's mass-to-charge acceptance, as shown in Fig. 2.

* sauerland@hiskp.uni-bonn.de

ISBN: 978-3-95450-212-7 ISSN: 2673-5482 doi:10.18429/JACoW-CYCLOTRONS2022-MOB003

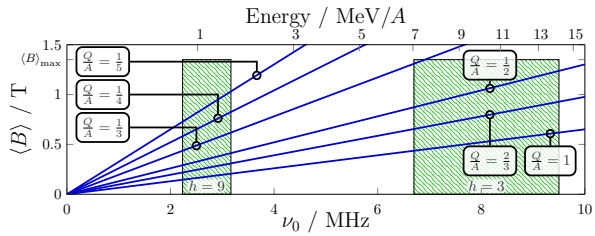

Figure 2: Parameter space of possible cyclotron operation (green) with average magnetic flux density $\langle B \rangle$ and ν_0.

After approx. 120 revolutions, the beam is extracted to a field-compensated channel in a single-turn extraction, using an electrostatic septum. The extracted beam can either be guided to the high current site, used to produce induced radioactivity in target material, or it is transported to the experimental sites via the high-energy beamline, featuring a versatile double mono or achromator system [2].

IRRADIATION SITE

In the *C* beamline, at extraction 2a (comp. Fig. 1), a new site for proton irradiation of silicon (pixel) detectors has been installed [3], enabling the application of highly-uniform damage profiles. The site is shown in Fig. 3. A calibrated beam monitor is used for non-destructive, continuous beam diagnostics, which is situated directly upstream of the beam exit window. The experimental setup is positioned on an optical breadboard in front of the window, mounted on a rail system with a supporting structure made of aluminum profiles. The rail system allows to retract the setup along the beam axis, enabling the positioning of a Faraday cup (FC) for e.g. beam monitor calibration (see Fig. 3, top right) in front of the exit window, using a vertical linear stage. A *Chromox* scintillation screen, installed on top of the FC enables visual beam diagnostic. The site is complemented by a 19″ rack for installation of the readout electronics as well as other devices and provides external interfaces to the irradiation site.

Beam Monitor

The custom-made beam monitor, comprising a secondary electron monitor (SEM) module and a beam loss monitor (BLM) module, is shown in Fig. 4.

In the SEM module, the surface emission of low-energy secondary electrons (SE), upon impact of fast ions into matter, is used to measure the beam current and relative position. Here, the beam propagates through two 5 µm-thick, carbon-coated[1] Al foil pairs, which are segmented vertically (SEM R & L) and horizontally (SEM U & D). Removing emitted SE from the electrically-isolated SEM-foils, results in a current signal proportional to the incident ion beam current and kinetic energy. Therefore, pull electrodes are located in close proximity to each SEM-foil's surface, consisting of

[1] To anticipate surface carbonization in vacuum with time, ≈ 70 nm layer thickness

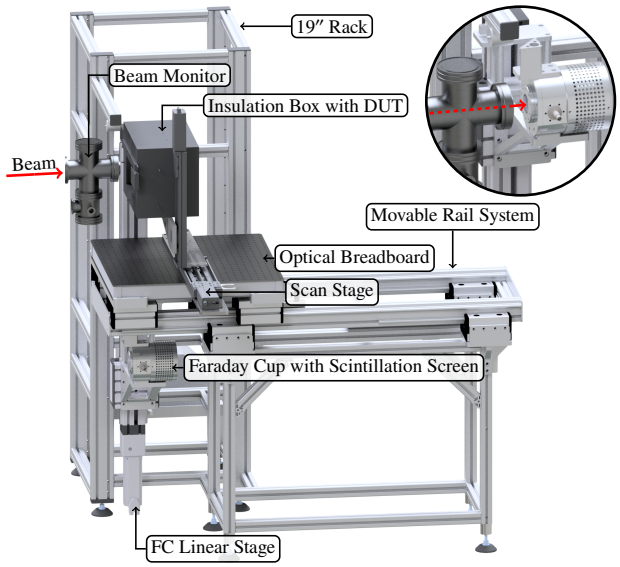

Figure 3: CAD render of the irradiation site. In the top right, beam monitor and Faraday cup are aligned for calibration.

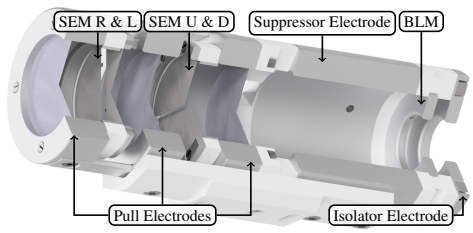

Figure 4: CAD render of a sectional view of the beam monitor with SEM (left) and BLM module (right).

three 5 µm-thick Al foils, biased with +100 V. After calibrating the SE to the ion beam current using the FC, the sum of all foil signals allows online measurement of the beam current whereas the foil-segmentation enables to determine the relative beam position.

The BLM module consist of a 3 mm-thick Al iris with a 20 mm diameter, mimicking the dimensions of the exit window, as well as two suppressor electrodes positioned in front of and behind the iris. Upon ion impact on the BLM iris, a current is flowing, indicating beam-truncation at the exit window. To prevent charge-loss due to SE emission, the suppressor electrodes are biased with −100 V.

Using the information provided by the BLM as well as the calibrated SEM, the beam monitor enables to determine the beam current which is extracted to the irradiation site. The beam monitor is designed utilizing the `Electrostatic` and `Particle in Cell (PIC) Solver` of `CST Studio Suite` to maximize the SE collection from the SEM-foils. A scenario with a 13.6 MeV proton beam is shown in Fig. 5. Here, SE trajectories are simulated, based on the potential of the electrodes and the SE-generated space charge. The SE yield (SEY) due to proton impact is calculated on basis of measurements of [4]. According to [5], the downstream SEY is approx. twice as large as upstream, for high-energy protons. The SE emission energy probability density func-

ISBN: 978-3-95450-212-7 ISSN: 2673-5482 doi:10.18429/JACoW-CYCLOTRONS2022-MOB003

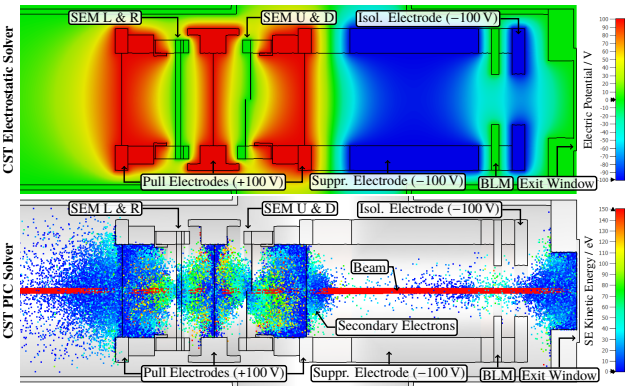

Figure 5: CST simulations: Electric potential of the beam monitor (top). Spatial distribution of SE for a proton beam current of 1 µA in its equilibrium state (bottom).

tion is a gamma distribution with an estimated mean energy of 15 eV, based on measurements of [6]. For this scenario, the resulting SE collection efficiency for both SEM-foils is (99.11 ± 0.19)% (upstream) and (99.77 ± 0.04)% (downstream).

Faraday Cup

The in-house developed Faraday cup, used for calibration of the beam monitor, is shown in Fig. 6.

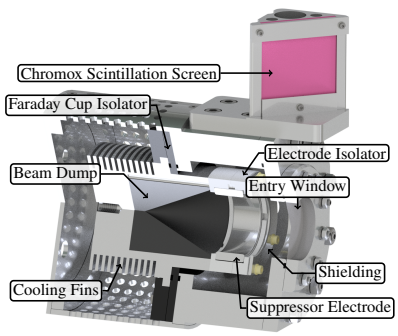

Figure 6: CAD render of a sectional view of the Faraday cup.

When positioned in front of the exit window, the beam enters the FC's vacuum system through a 30 µm thick AlMg3 entry window and impinges on the graphite beam dump after passing through a cylindrical suppressor electrode ring. The beam dump has an inverted cone-shape, preventing the majority of SE to escape, as their emission angle in reference to the surface normal is a cosine probability distribution with its maximum at an angle parallel to surface normal. For SE with unfavorable emission angles, the suppressor electrodes potential barrier, biased with typ. −100 V, repels them back into the cup (see Fig. 7 (left)).

The Faraday cup's inner geometry is designed to prevent an escape of the majority of emitted SE out of the cup also using CST. With identical SEY and SE emission energy probability density function as in the beam monitor simulations, the SE distribution in its equilibrium state is shown in Fig. 7 (right) for an impinging 13.6 MeV proton beam with a current of 1 µA. In this scenario, the relative SE escape ratio of the FC is 7.6×10^{-5}.

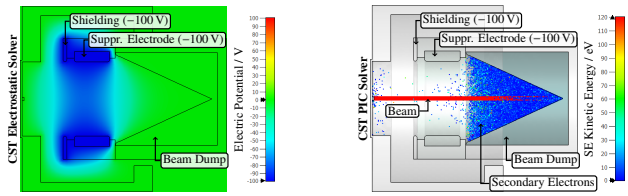

Figure 7: CST simulations: Electric potential of the Faraday cup (left). Spatial distribution of SE for a proton beam current of 1 µA in its equilibrium state (right).

Calibration

In the top-right of Fig. 3, the configuration of the site for beam monitor calibration is depicted. The beam traverses the beam monitor and is subsequently extracted into the FC. The sum of the SEM module foil currents I_Σ is calibrated against the beam current I_{beam} measured in the FC. The calibration factor is defined as $\lambda = \beta/5\,\text{V}$ with $\beta = I_{\text{beam}}/I_\Sigma$ and can be obtained by varying the incident beam current as shown in Fig. 8. This allows to determine the beam current I_{beam} online, as a function of the SEM module signals and data acquisition parameters. λ is proportional to the SEY for 100 % SE collection efficiency in the beam monitor and thus depends on the ion species, used for the irradiation, and its kinetic energy.

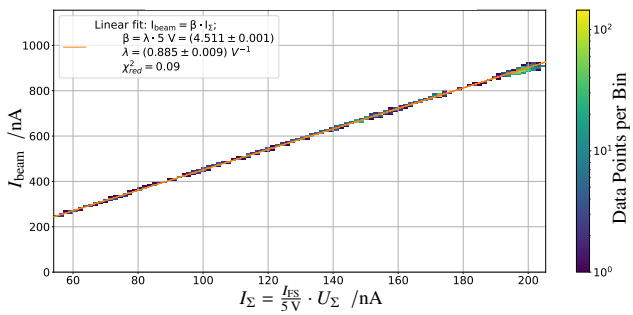

Figure 8: Calibration of the beam monitor using the FC.

DUT IRRADIATION

A 14 MeV proton beam is used to irradiate DUTs, housed in a thermally-insulated cooling box (comp. Fig. 3). The box fits DUTs with a maximum size of 19 × 11 cm^2 and is attached to a scan stage, which has a range of 30 cm × 30 cm. Typically, DUTs are mounted behind a customized, 6 mm-thick Al shielding, exposing only the DUT to the beam. A scintillation screen on the shielding allows for an optical, beam-based alignment of the setup. To prevent annealing during irradiation, a temperature of < −20 °C is maintained at the DUT by guiding cool nitrogen gas onto the irradiated area. To ensure uniform irradiation profiles, the scan stage is used to move the DUT on a row-based grid through the beam (see Fig. 9).

ISBN: 978-3-95450-212-7 ISSN: 2673-5482 doi:10.18429/JACoW-CYCLOTRONS2022-MOB003

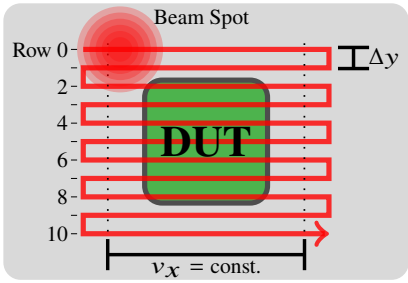

Figure 9: Relative movement of the beam along the scan pattern over the DUT (green) and the shielding (gray).

DAQ and Control

A custom-made analog readout board is used to convert the current signals from the beam monitor and the FC to voltages according to $U_{\text{out}} = 5\,\text{V}/I_{\text{FS}} \cdot I_{\text{in}}$. To resolve different magnitudes of currents, the board features several gain settings, corresponding to full-scale currents I_{FS} between 50 nA to 100 µA. In addition to the conversion, the ±5 V-normalized analog sum of the SEM foil signals U_{Σ} is generated, serving as the calibration signal.

Typically, one or more *Raspberry Pi* single-board computers are used as servers to interface the setup and collect irradiation-relevant data. Through these servers, the *Python* package `irrad_control` [7] provides full setup control, data acquisition and analysis. The software features online data visualization and interpretation with graphical user interface, allowing a beam-driven irradiation procedure as well as post-irradiation corrections, resulting in highly-uniform damage distributions.

Beam-Driven Irradiation Procedure

To ensure a uniform particle fluence distribution, an area larger than the DUT is defined and divided into a row-based grid (see Fig. 9). In this scan pattern, the DUT is repeatedly moved along the rows through the beam, with the turning points located off the DUT on an Al shielding. A constant scan velocity v_x and a row separation Δy smaller than the beam diameter allow to unfold the beam's transversal charge distribution homogeneously onto the DUT area. Online measurement of the beam parameters enables a beam-driven procedure: beam characteristics (e.g. current, position and stability) are probed against predefined requirements at the turning points, before scanning a row. Consequently, the scan parameters are adapted or the procedure is paused off DUT until conditions suffice. This autonomous procedure results in highly-uniform fluence distributions.

Fluence Distribution and Error Estimation

Extensive data acquisition of the setup components during irradiation enables to generate particle fluence distributions across the scan area. A typical fluence distribution is shown in Fig. 10. In the central region, containing the DUT, the fluence is applied homogeneously. In contrast, the turning point regions, located at the opposite ends of the area, are exposed to a higher fluence due to the turning itself as well as irradiation pauses, initiated by the beam-driven irradiation procedure. The variance of the proton fluence within the homogeneous region is insignificant with respect to its relative uncertainty of typically 2%. It is composed of the individual error on the beam monitor calibration and the readout board accuracy.

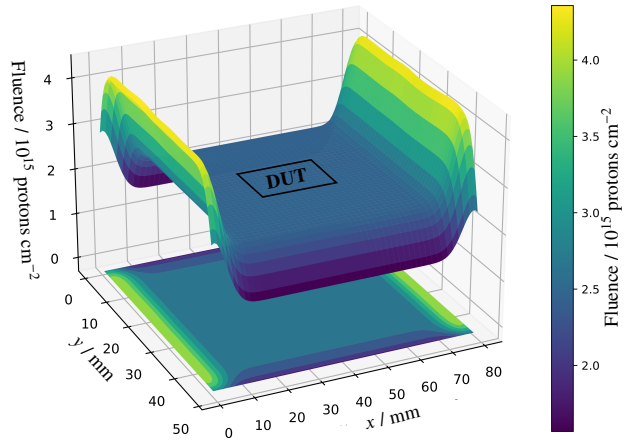

Figure 10: Typical fluence distribution on the scan area for a DUT aim fluence of $2.5 \cdot 10^{15}$ protons cm^{-2}.

REFERENCES

[1] "The AEG isochronous cyclotron at the University of Bonn", *IEEE Trans. Nucl. Sci.*, vol. 13, no. 4, pp. 435–436, 1966. doi:10.1109/TNS.1966.4324267

[2] F. Hinterberger *et al.*, "The beam handling system at the Bonn isochronous cyclotron", *Nucl. Instrum. Methods*, vol. 130, pp. 335–346, 1975. doi:10.1016/0029-554X(75)90033-6

[3] D. Sauerland *et al.*, "Proton irradiation site for Si-detectors at the Bonn Isochronous Cyclotron", in *Proc. IPAC'22*, Bangkok, Thailand, Jun. 2022, pp. 130–132. doi:10.18429/JACoW-IPAC2022-MOPOST030

[4] H. P. Beck and R. Langkau, "Die Sekundärelektronen-Ausbeute verschiedener Materialien bei Beschuß mit leichten Ionen hoher Energie", *Zeitung für Naturforschung A*, vol. 30, no. 8, pp. 981-985, 1975. doi:10.1515/zna-1975-0810

[5] E. F. Da Silveira and J. M. F. Jeronymo, "Secondary electron emission from the entrance and exit surfaces of thin aluminium foils under fast light ion bombardment", *Nucl. Instrum. Methods Phys. Res. Sect. B*, vol. 24-25, part 1, pp. 534–537, 1987. doi:10.1016/0168-583X(87)90702-6

[6] H. Rothard, K. O. Groeneveld, and J. Kemmler, "Kinetic Electron Emission from Ion Penetration of Thin Foils in Relation to the Pre-Equilibrium of Charge Distributions", *Particle Induced Electron Emission II*, Springer Verlag, 1992.

[7] P. Wolf, "irrad_control: Control, DAQ and Analysis Software for the Irradiation Site at the Bonn Cyclotron", https://github.com/Cyclotron-Bonn/irrad_control